Frontiers of Information Technology & Electronic Engineering
www.jzus.zju.edu.cn; engineering.cae.cn; www.springerlink.com
ISSN 2095-9184 (print); ISSN 2095-9230 (online)
E-mail: jzus@zju.edu.cn

Comprehensive evaluation factor of optoelectronic properties for transparent conductive metallic mesh films*

Yilei ZHANG[1,2], Jinxuan CAO[1,2], Zhengang LU[†‡1,2], Heyan WANG[1,2], Jiubin TAN[1,2]

[1]*Center of Ultra-precision Optoelectronic Instrument Engineering, Harbin Institute of Technology, Harbin 150080, China*

[2]*Key Lab of Ultra-precision Intelligent Instrumentation (Harbin Institute of Technology), Ministry of Industry and Information Technology, Harbin 150080, China*

[†]E-mail: luzhengang@hit.edu.cn

Received Dec. 10, 2020; Revision accepted Mar. 30, 2021; Crosschecked Oct. 12, 2021

Abstract: Finding the optimal optoelectronic properties (zero-order optical transmittance, shielding effectiveness, and stray light uniformity) of metallic mesh is significant for its application in electromagnetic interference shielding areas. However, there are few relevant studies at present. Based on optoelectronic properties, we propose a comprehensive evaluation factor Q, which is simple in form and can be used to evaluate the mesh with different parameters in a simple and efficient way. The effectivity of Q is verified by comparing the trend of Q values with the evaluation results of the technique for order preference by similarity to ideal solution (TOPSIS). The evaluation factor Q can also be extended to evaluate the optoelectronic properties of different kinds of metallic meshes, which makes it extremely favorable for metallic mesh design and application.

Key words: Metallic mesh; Technique for order preference by similarity to ideal solution (TOPSIS); Entropy weight (EW); Comprehensive evaluation; Transparent conductive films

https://doi.org/10.1631/FITEE.2000690 **CLC number:** TN713; O441; O484

1 Introduction

With the rapid development of wireless communication technology (Palmer, 2019; Gao et al., 2020; Zhang XX et al., 2020), the electromagnetic environment grows increasingly complex and the need for electromagnetic interference (EMI) shielding is increasingly urgent. EMI shielding of optical transparent windows and components is extremely difficult as there exist inherent conflicts between the high optical transmittance and strong shielding effectiveness (SE) (Lu ZG et al., 2014; Polley et al., 2014; Wen et al., 2014; Wang HY et al., 2017, 2018). Transparent conductors are one of the most effective methods for EMI shielding for optical transparent elements, and include the metal oxide based transparent conductors (such as ZnO and ITO) (Kim et al., 2005; Zhu M et al., 2007; Greco et al., 2008; Yamada et al., 2008), carbon-based structures (such as nanotube arrays and graphene films) (Wu ZC et al., 2004; Hecht et al., 2011; Hong et al., 2012; Khrapach et al., 2012; Han et al., 2015; Zhu HX et al., 2019), and metallic networks (such as metallic meshes and silver nanowires) (Kohin et al., 1993; Halman et al., 2009; Madaria et al., 2010; Zeng et al., 2010; Murray et al., 2011; Lu ZG et al., 2014, 2016; Wang HY et al., 2016, 2017, 2018; Wang WQ et al., 2018; Zhu HX et al., 2019; Wu and Cui, 2020; Zhong et al., 2020). Metallic meshes can achieve wideband optical transmittance from the visible to infrared bands, and their use is one of the research hot spots in the field of transparent

‡ Corresponding author

* Project supported by the National Natural Science Foundation of China (No. 61975046)

ORCID: Yilei ZHANG, https://orcid.org/0000-0003-0133-4128; Zhengang LU, https://orcid.org/0000-0001-6490-5819; Heyan WANG, https://orcid.org/0000-0003-1740-4565

EMI shielding. However, the concentrated stray light caused by mesh diffraction is a serious drawback of these meshes. At present, there are many novel metallic mesh structures which produce a uniform diffraction distribution of stray light (Halman et al., 2009; Murray et al., 2011; Lu ZG et al., 2014, 2016; Wang HY et al., 2016, 2017, 2018; Wang WQ et al., 2018; Zhong et al., 2020). Different meshes have different diffraction characteristics. However, EMI SE and optical transmittance of metallic meshes are mutually restricted. Therefore, to achieve optimal optoelectronic properties (EMI SE, optical transmittance, and stray light uniformity) for metallic meshes, it is necessary to conduct a comprehensive evaluation with different parameters based on these optoelectronic properties. However, so far there have been few studies on this aspect.

In this study, given the contradicting aspects of optoelectronic properties mentioned above in the metallic mesh, a comprehensive evaluation factor Q is proposed to evaluate the optoelectronic properties. The typical comprehensive evaluation (CE) process of the technique for order preference by similarity to ideal solution (TOPSIS) based on the entropy weight (EW), which has no strict rules and is suitable for evaluating multiple criteria, is used to verify the validity of Q. In addition, we use Q to describe five different mesh structures. We show that Q can be further extended to evaluate the performance of different metallic meshes. Therefore, this comprehensive evaluation method should be of great significance for metallic mesh design and application, since it can be used to obtain the optimal mesh structure and mesh parameters, providing a time-saving and cost-efficient method for optoelectronic property evaluation of the metallic mesh.

2 Contradiction analysis of optoelectronic properties for the metallic mesh

For a mesh, there is a close link between structural parameters and optoelectronic properties. The main structural parameters of the mesh are its period and fabricated linewidth, i.e., g and $2a$ respectively, as shown in Fig. 1a, for the most typical single-layer square metallic mesh (SSMM). These determine the main optoelectronic properties, including EMI SE, optical transmittance or zero-order optical transmittance, and stray light uniformity.

According to the classical metallic mesh analytical models (Kohin et al., 1993; Tan and Lu, 2007; Tan and Liu, 2008), zero-order optical transmittance, EMI SE, and stray light uniformity of the SSMM are calculated as shown in Figs. 1b–1d. From the scalar diffraction theory, zero-order optical transmittance of a mesh is the square of its total optical transmittance. The total optical transmittance is approximately the ratio of the non-metal covered area to the total area. However, in visual imaging application, only the zero-order light is favorable for imaging, while other high-order diffraction light contributes to stray light, which can degrade image quality and the signal-to-noise ratio. Therefore, zero-order optical transmittance is used to evaluate optical transmission characteristics.

Since stray light cannot be eliminated, the high-order diffraction energy should be distributed as uniformly as possible. The stray light uniformity U is defined as the whole intensity of stray light divided by the maximum of high-order diffraction intensity. According to the relationship between stray light and zero-order optical transmittance, the whole intensity of stray light X can be expressed as follows:

$$X = I\left(\sqrt{T_0} - T_0\right), \tag{1}$$

where I is the incident optical intensity, T_0 is the zero-order optical transmittance, and $\sqrt{T_0}$ is the total optical transmittance. Thus, $I\left(\sqrt{T_0} - T_0\right)$ represents the whole intensity of stray light.

The stray light uniformity U can be expressed as

$$U = \frac{X}{DI} = \frac{I\left(\sqrt{T_0} - T_0\right)}{DI} = \frac{\sqrt{T_0} - T_0}{D}, \tag{2}$$

where D is the maximum of the normalized high-order diffraction. According to Eq. (2), the increase of U means that the proportion of D in the whole stray light intensity decreases, indicating that the stray light is more uniform. Here, we use U to evaluate the diffraction characteristics of metallic meshes.

Fig. 1 shows that with the decrease of linewidth $2a$ or the increase of period g, zero-order optical

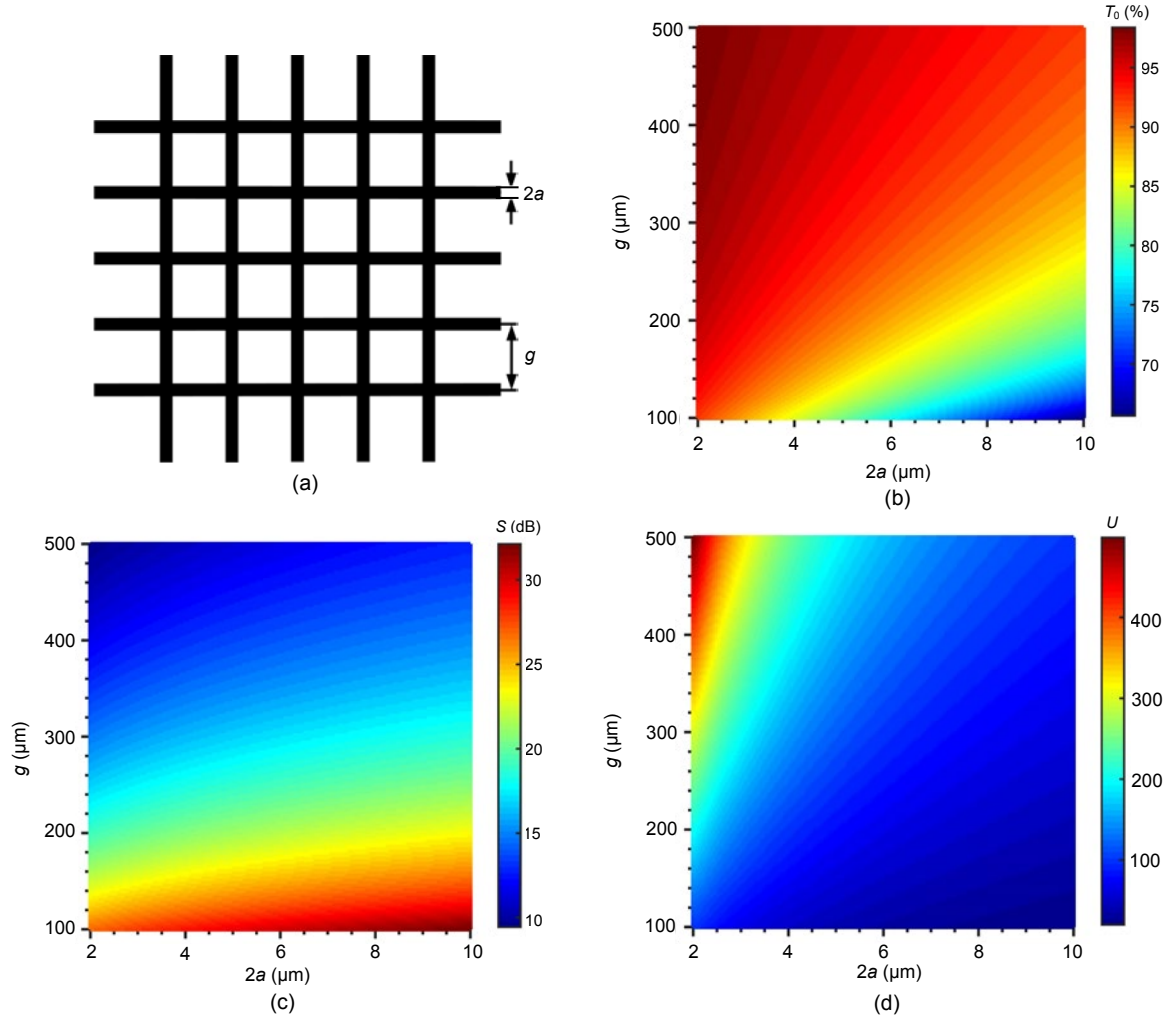

Fig. 1 Diagram of the square metallic mesh (a) and relationships between the optoelectronic properties and the structural parameters of SSMM: zero-order optical transmittance (b); EMI SE (c); stray light uniformity (d)

transmittance and stray light uniformity decrease, which is beneficial to imaging applications. However, the trend of EMI SE is opposite to that of zero-order optical transmittance. Because the ideal metallic mesh would achieve strong EMI SE, high zero-order optical transmittance, and good stray light uniformity simultaneously, there is a conflict between EMI SE and zero-order optical transmittance in the selection of mesh structural parameters.

In addition, under the premise of the same light transmittance, SE and stray light uniformity of different meshes can vary greatly. Therefore, it is necessary to design a comprehensive evaluation factor for optoelectronic properties, so as to achieve an optimal balance in its performance.

3 Comprehensive evaluation factor *Q* for optoelectronic properties of the metallic mesh

To evaluate the quality of different mesh structures and parameters, based on the above three important optoelectronic properties, we propose a CE standard by defining a comprehensive evaluation factor Q, similar to the "quality factor" in the circuit and factor Q in the literature (Rhodes, 1972; Horng et al., 2003; Vorobyev, 2011). Q is expressed as follows:

$$Q=\sqrt{T_0}SU, \tag{3}$$

where S is the EMI SE. T_0, S, and U can be obtained

by experimental measurement or calculated by the specific mesh period and linewidth. From the analysis in Section 2, the larger the values of T_0, S, and U, the better the mesh. Therefore, the larger the value of Q, the better the optoelectronic performance. Since the form of Q is simple, optoelectronic properties of any metallic mesh can be evaluated rapidly.

Next, we take SSMM as an example and use a typical CE method TOPSTIS to evaluate it. The result can be compared with the value of Q to verify its validity.

4 TOPSIS comprehensive evaluation method based on the entropy weight

TOPSIS is a typical CE method and has no strict rules on the number of samples and the number of criteria or the distribution of data (Jahanshahloo et al., 2006; Shih et al., 2007; Yang and Hung, 2007; Krohling et al., 2015; Kuo, 2017). Because the metallic mesh has three important optoelectronic properties, TOPSIS is suitable for solving this complex multi-criterion evaluation problem. TOPSIS evaluates the properties of the alternatives through the similarity to the ideal solution. In the evaluation process, the relative weight of each criterion is determined objectively by EW, making the final evaluation result more reasonable and credible.

The specific steps of TOPSIS based on EW for SSMM are shown in the following subsections.

4.1 Forming decision matrix

A decision matrix includes alternatives and criteria, and can be described by Eq. (4):

$$\boldsymbol{X}=\begin{array}{c|ccc} & \boldsymbol{C}_1 & \cdots & \boldsymbol{C}_n \\ \hline \boldsymbol{A}_1 & x_{11} & \cdots & x_{1n} \\ \vdots & \vdots & & \vdots \\ \boldsymbol{A}_m & x_{m1} & \cdots & x_{mn} \end{array}, \tag{4}$$

where $\boldsymbol{A}_1$–$\boldsymbol{A}_m$ are viable alternatives (m represents the number of different design parameters for the metallic mesh), $\boldsymbol{C}_1$–$\boldsymbol{C}_n$ are criteria, with the three important optoelectronic properties mentioned in Section 3 as the criteria, with C_1=T_0 (zero-order optical transmittance), C_2=S (EMI SE), and C_3=U (stray light uniformity), and x_{ij} indicates the value of $\boldsymbol{C}_j$ in the mesh alternative $\boldsymbol{A}_i$.

In general, the criteria are classified into two types: benefit and cost. The benefit criteria are such that a higher value is better, while for cost criteria, the opposite is the case. In engineering applications, zero-order optical transmittance, EMI SE, and stray light uniformity are all benefit criteria.

Metallic meshes with high optical transmittance (T_0≥90%) and strong shielding (S≥15 dB) are appropriate in most transparent EMI shielding applications. We evaluate this kind of SSMM in this part. According to the calculation models of Kohin et al. (1993), with the actual fabricated linewidth 2a not less than 2 μm as the constraint condition, the design parameter range of the SSMM with high optical transmittance and strong shielding (SSMM-HTSS) is shown in Fig. 2a. In this range, each pair of g and 2a for the SSMM satisfies the conditions of T_0≥90% and S≥15 dB. Therefore, these parameter ranges constitute the area to be evaluated. To present the entire information of the whole evaluated area and reduce the calculation time, sampling points are evenly distributed in the area, as shown in Fig. 2b. There are 109 sampling points in Fig. 2b. These are the alternatives $\boldsymbol{A}_1, \boldsymbol{A}_2, ..., \boldsymbol{A}_m$ in the decision matrix (4). The sampling linewidth and period interval are 0.5 and 20 μm, respectively. Then all the evaluation criteria of different alternatives are calculated. Evaluation criteria for the alternatives when 2a=2 μm are shown in Table 1.

4.2 Normalizing the decision matrix

For the next step, the evaluation criteria of viable alternatives need to be turned into a comparable scale

Table 1 Evaluation criteria for alternatives of SSMM when 2a=2 μm

Alternative number	T_0 (%)	S (dB)	U	2a (μm)	g (μm)
1	92.24	26.718	99.13	2	100
2	93.50	24.689	119.11	2	120
3	94.41	22.990	139.09	2	140
4	95.09	21.530	159.08	2	160
5	95.63	20.250	179.07	2	180
6	96.06	19.112	199.07	2	200
7	96.41	18.087	219.06	2	220
8	96.71	17.155	239.05	2	240
9	96.96	16.301	259.05	2	260
10	97.17	15.513	279.05	2	280

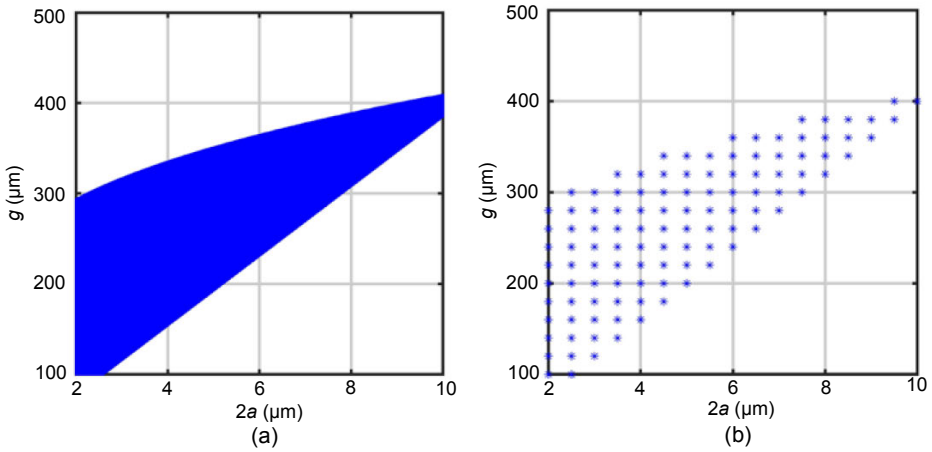

Fig. 2 Evaluation area (a) and evenly distributed sampling points (b) of SSMM-HTSS

by normalization. The normalized decision matrix $\boldsymbol{H}=(h_{ij})_{m\times n}$ is calculated as

$$h_{ij}=\frac{x_{ij}}{\sqrt{\sum_{i=1}^{m}(x_{ij})^2}},\ i=1,2,\cdots,m,\ \ j=1,2,\cdots,n. \quad (5)$$

4.3 Constructing the weighted decision matrix by the entropy weight

EW is an objective weighting method (Zou et al., 2006; Zhang H et al., 2011; Ji et al., 2015), and the specific calculation steps are shown as follows:

First, the standardized matrix $\boldsymbol{V}=(v_{ij})_{m\times n}$ is obtained by standardizing the decision matrix $\boldsymbol{X}$, which is shown in Eq. (6):

$$v_{ij}=\begin{cases}\dfrac{x_{ij}-\min(x_j)}{\max(x_j)-\min(x_j)}, & \text{benefit criteria,}\\ \dfrac{\max(x_j)-x_{ij}}{\max(x_j)-\min(x_j)}, & \text{cost criteria.}\end{cases} \quad (6)$$

From the standardized matrix $\boldsymbol{V}$, the information entropy of the j^{th} criterion is defined as

$$e_j=-\frac{1}{\ln m}\sum_{i=1}^{m}p_{ij}\ln p_{ij}, \quad (7)$$

where

$$p_{ij}=\frac{v_{ij}}{\sum_{i=1}^{m}v_{ij}}. \quad (8)$$

From the concept of entropy, the greater the deviation degree of the j^{th} criterion is, the more information the criterion provides and the greater the weight of the j^{th} criterion is.

The weight of entropy for the j^{th} criterion could be defined as w_j, which forms the criterion weight matrix $\boldsymbol{W}=(w_j)_{1\times n}$:

$$w_j=\frac{1-e_j}{n-\sum_{j=1}^{n}e_j},\qquad j=1,2,\cdots,n. \quad (9)$$

From Eqs. (6)–(9), the objective entropy weight of the sample points is obtained. This is the relative weight of the evaluation criteria of SSMM-HTSS:

$$T_0:S:D=0.2724:0.3037:0.4239. \quad (10)$$

The weighted decision matrix on the basis of EW is constructed by multiplying the criterion weight matrix $\boldsymbol{W}$ by the normalized decision matrix $\boldsymbol{H}$ obtained in Section 4.2. The weighted decision matrix $\boldsymbol{R}=(r_{ij})_{m\times n}$ can be expressed as

$$r_{ij}=w_jh_{ij},\ \ i=1,2,\cdots,m,\ j=1,2,\cdots,n. \quad (11)$$

4.4 Determining the positive ideal solution S_j^+ and negative ideal solution S_j^-

In this subsection, S_j^+ and S_j^- can be obtained as the basis for calculating the separation. S_j^+ indicates the most preferable alternative, while S_j^- indicates the

least preferable alternative. S_j^+ and S_j^- are defined in terms of the weighted decision values, as shown in Eqs. (12) and (13), respectively:

$$S_j^+ = \left\{r_1^+, r_2^+, \cdots, r_n^+\right\} = \left\{(\max_i(r_{ij})|j\in J_1), (\min_i(r_{ij})|j\in J_2)|i=1,\cdots,m\right\}, \tag{12}$$

$$S_j^- = \left\{r_1^-, r_2^-, \cdots, r_n^-\right\} = \left\{(\min_i(r_{ij})|j\in J_1), (\max_i(r_{ij})|j\in J_2)|i=1,\cdots,m\right\}, \tag{13}$$

where J_1 is associated with benefit criteria and J_2 is associated with cost criteria.

4.5 Calculating the separation

The separation between alternatives can be calculated by the n-dimensional Euclidean distance. The separation of each alternative from S_j^+ is given as

$$\mathrm{Sd}_i^+ = \sqrt{\sum_{j=1}^{n}\left(S_j^+ - r_{ij}\right)^2},\ i=1,2,\cdots,m. \tag{14}$$

Similarly, the separation of each alternative from S_j^- is given as

$$\mathrm{Sd}_i^- = \sqrt{\sum_{j=1}^{n}\left(S_j^- - r_{ij}\right)^2},\ i=1,2,\cdots,m. \tag{15}$$

4.6 Calculating the relative closeness to the ideal solution

The relative closeness of each viable alternative to the ideal solution S_j^+ is defined as η_i in Eq. (16). The viable alternative is closer to the ideal solution with increasing η_i, which indicates a better evaluation result.

$$\eta_i = \frac{\mathrm{Sd}_i^-}{\mathrm{Sd}_i^+ + \mathrm{Sd}_i^-},\ i=1,2,\cdots,m. \tag{16}$$

From Eqs. (11)–(16), the relative closeness of 109 alternatives is obtained (Fig. 3). It can be seen that as the period increases, the relative closeness increases as well. When the period is similar, the relative closeness of each alternative decreases with the increase of the linewidth. In brief, the largest period with the smallest linewidth for SSMM-HTSS reveals the best CE result. In addition, the optimal design parameters of SSMM-HTSS can be found at the position of the highest relative closeness value in Fig. 3: linewidth $2a$=2 μm and period g=280 μm. The corresponding optimal comprehensive optoelectronic properties are T_0=97.17%, S=15.513 dB, and U=279.0468.

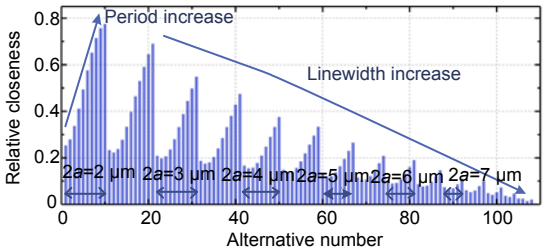

Fig. 3 Relative closeness bar chart of 109 SSMM-HTSS alternatives

For SSMM-HTSS, the relative closeness of mesh alternatives and the value of Q are compared under different design parameters, as shown in Fig. 4. The trend of the Q value agrees well with that of relative closeness, which shows that Q can represent the optoelectronic properties of the metallic meshes effectively.

5 Comparative evaluation of five different metallic meshes

The comprehensive evaluation factor Q can be used not only to evaluate different parameters of one kind of metallic mesh, but also to compare metallic meshes with different structures under various parameters. Table 2 shows the values of T_0, S, U, and evaluation factor Q of the five reported metallic meshes under the same fabricated linewidth (3.5 μm) and zero-order optical transmittance (T_0=90.25%).

It can be seen that the value of evaluation factor Q for the ring metallic mesh is higher than that of the square metallic mesh. This indicates that the ring metallic mesh has better optoelectronic properties than the square metallic mesh, which is consistent with existing research findings (Tan and Lu, 2007). In addition, the values of Q for various complex metallic meshes in the literature designed to homogenize stray

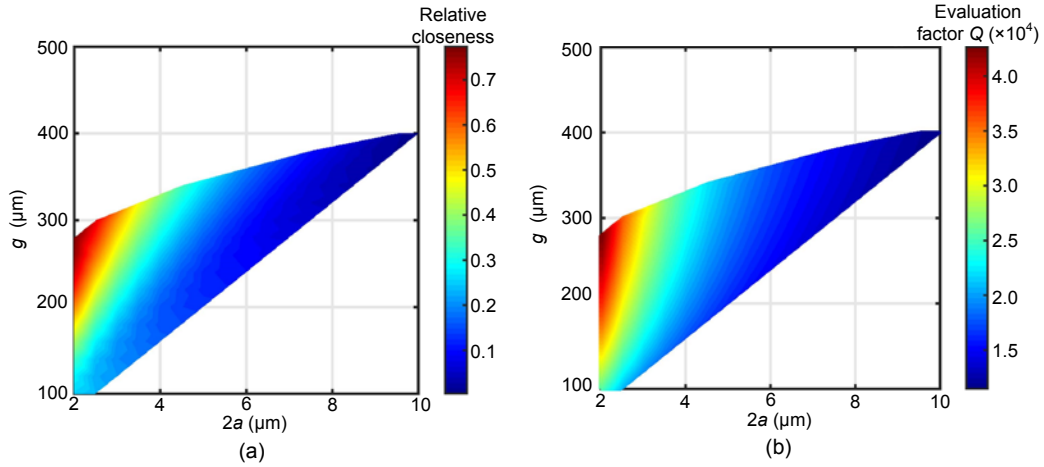

Fig. 4 Relationship between relative closeness and the design parameters of SSMM-HTSS (a) and between evaluation factor *Q* and the design parameters of SSMM-HTSS (b)

Table 2 Comprehensive evaluation factor *Q* for five different metallic meshes

Metallic mesh	T_0 (%)	S (dB)	U	Q	Reference
Square metallic mesh	90.25	26.92	102.26	2484.437	Kohin et al. (1993)
Ring metallic mesh	90.25	22.08	225.78	4499.163	Tan and Lu (2007)
Nested multi-ring array metallic mesh	90.25	20.13	535.42	9727.149	Wang HY et al. (2017)
Triangular ring mesh with rotated sub-rings	90.25	20.69	670.96	12 528.65	Lu ZG et al. (2016)
Interlaced multi-ring metallic mesh	90.25	21.42	960.93	18 576.27	Lu X et al. (2019)

light are higher than that of the ring metallic mesh. The interlaced multi-ring metallic mesh has the highest value of Q among the five different metallic meshes (Lu X et al., 2019). Therefore, Q is applicable for evaluation of differently shaped meshes, providing guidance for the selection of mesh types in engineering applications.

6 Conclusions

In this paper, we proposed a comprehensive evaluation factor Q constructed from the three main criteria for metallic mesh, i.e., zero-order optical transmittance, EMI SE, and stray light uniformity. Q can be used to quantitatively evaluate the optoelectronic properties of the metallic mesh with different parameters. The trend of the relative closeness obtained by evaluating the SSMM using the method of TOPSIS based on EW agreed well with the trend of Q, which shows the efficacy of Q. We also used Q to evaluate five different metallic meshes at the same fabricated linewidth and optical transmittance, which shows that Q is suitable for evaluating meshes with different shapes. Q can be extended to the application to the evaluation of multi-layer meshes. Because of its simple form and direct relation to optoelectronic property criteria, Q can be used to evaluate the optoelectronic properties of meshes with any structure or parameters quickly and comprehensively. Thus, it should be of great significance in the design and application of conductive metallic meshes.

Contributors

Zhengang LU designed the research. Yilei ZHANG performed the simulations and drafted the manuscript. Jinxuan CAO processed the data and gave suggestions for the verification methods. Heyan WANG and Jiubin TAN helped organize the manuscript. Yilei ZHANG and Zhengang LU revised and finalized the paper.

Compliance with ethics guidelines

Yilei ZHANG, Jinxuan CAO, Zhengang LU, Heyan WANG, and Jiubin TAN declare that they have no conflict of interest.

References

Gao F, Gao P, Zhu WT, et al., 2020. 5G evolution promoting innovation of antenna systems. *Front Inform Technol Electron Eng*, 21(1):188-194.

https://doi.org/10.1631/FITEE.1900561

Greco S, Sarto MS, Tamburrano A, 2008. Shielding performances of ITO transparent windows: theoretical and experimental characterization. Proc Int Symp on Electromagnetic Compatibility-EMC Europe, p.1-6. https://doi.org/10.1109/EMCEUROPE.2008.4786870

Halman JI, Ramsey KA, Thomas M, et al., 2009. Predicted and measured transmission and diffraction by a metallic mesh coating. Proc SPIE 7302, Window and Dome Technologies and Materials XI, Article 73020Y. https://doi.org/10.1117/12.818760

Han JC, Wang XN, Qiu YF, et al., 2015. Infrared-transparent films based on conductive graphene network fabrics for electromagnetic shielding. *Carbon*, 87:206-214. https://doi.org/10.1016/j.carbon.2015.01.057

Hecht DS, Hu LB, Irvin G, 2011. Emerging transparent electrodes based on thin films of carbon nanotubes, graphene, and metallic nanostructures. *Adv Mater*, 23(13):1482-1513. https://doi.org/10.1002/adma.201003188

Hong SK, Kim KY, Kim TY, et al., 2012. Electromagnetic interference shielding effectiveness of monolayer graphene. *Nanotechnology*, 23(45):455704. https://doi.org/10.1088/0957-4484/23/45/455704

Horng TS, Peng KC, Jau JK, et al., 2003. S-parameter formulation of quality factor for a spiral inductor in generalized two-port configuration. *IEEE Trans Microw Theory Techn*, 51(11):2197-2202. https://doi.org/10.1109/TMTT.2003.818584

Jahanshahloo GR, Lotfi FH, Izadikhah M, 2006. An algorithmic method to extend TOPSIS for decision-making problems with interval data. *Appl Math Comput*, 175(2):1375-1384. https://doi.org/10.1016/j.amc.2005.08.048

Ji Y, Huang GH, Sun W, 2015. Risk assessment of hydropower stations through an integrated fuzzy entropy-weight multiple criteria decision making method: a case study of the Xiangxi River. *Expert Syst Appl*, 42(12):5380-5389. https://doi.org/10.1016/j.eswa.2014.12.026

Khrapach I, Withers F, Bointon TH, et al., 2012. Novel highly conductive and transparent graphene-based conductors. *Adv Mater*, 24(21):2844-2849. https://doi.org/10.1002/adma.201200489

Kim WM, Ku DY, Lee IK, et al., 2005. The electromagnetic interference shielding effect of indium–zinc oxide/silver alloy multilayered thin films. *Thin Sol Films*, 473(2):315-320. https://doi.org/10.1016/j.tsf.2004.08.083

Kohin M, Wein SJ, Traylor JD, et al., 1993. Analysis and design of transparent conductive coatings and filters. *Opt Eng*, 32(5):911-925. https://doi.org/10.1117/12.130266

Krohling RA, Lourenzutti R, Campos M, 2015. Ranking and comparing evolutionary algorithms with Hellinger-TOPSIS. *Appl Soft Comput*, 37:217-226. https://doi.org/10.1016/j.asoc.2015.08.012

Kuo T, 2017. A modified TOPSIS with a different ranking index. *Eur J Oper Res*, 260(1):152-160. https://doi.org/10.1016/j.ejor.2016.11.052

Lu X, Liu YS, Lu ZG, et al., 2019. High-transmittance double-layer frequency-selective surface based on interlaced multiring metallic mesh. *Opt Lett*, 44(5):1253-1256. https://doi.org/10.1364/OL.44.001253

Lu ZG, Wang HY, Tan JB, et al., 2014. Microwave shielding enhancement of high-transparency, double-layer, submillimeter-period metallic mesh. *Appl Phys Lett*, 105(24):241904. https://doi.org/10.1063/1.4904466

Lu ZG, Wang HY, Tan JB, et al., 2016. Achieving an ultra-uniform diffraction pattern of stray light with metallic meshes by using ring and sub-ring arrays. *Opt Lett*, 41(9):1941-1944. https://doi.org/10.1364/OL.41.001941

Madaria AR, Kumar A, Ishikawa FN, et al., 2010. Uniform, highly conductive, and patterned transparent films of a percolating silver nanowire network on rigid and flexible substrates using a dry transfer technique. *Nano Res*, 3(8):564-573. https://doi.org/10.1007/s12274-010-0017-5

Murray IB, Densmore V, Bora V, et al., 2011. Numerical comparison of grid pattern diffraction effects through measurement and modeling with OptiScan software. Proc SPIE 8016, Window and Dome Technologies and Materials XII, Article 80160U. https://doi.org/10.1117/12.883422

Palmer C, 2019. A storm over potential 5G interference. *Engineering*, 5(5):815-816. https://doi.org/10.1016/j.eng.2019.08.007

Polley D, Barman A, Mitra RK, 2014. EMI shielding and conductivity of carbon nanotube-polymer composites at terahertz frequency. *Opt Lett*, 39(6):1541-1544. https://doi.org/10.1364/OL.39.001541

Rhodes DR, 1972. On the quality factor of strip and line source antennas and its relationship to superdirectivity ratio. *IEEE Trans Antenn Propag*, 20(3):318-325. https://doi.org/10.1109/TAP.1972.1140191

Shih HS, Shyur HJ, Lee ES, 2007. An extension of TOPSIS for group decision making. *Math Comput Model*, 45(7-8):801-813. https://doi.org/10.1016/j.mcm.2006.03.023

Tan JB, Liu YM, 2008. Optimization of optical communication window mesh through full-wave analysis of periodic mesh. *Opt Commun*, 281(19):4835-4839. https://doi.org/10.1016/j.optcom.2008.06.044

Tan JB, Lu ZG, 2007. Contiguous metallic rings: an inductive mesh with high transmissivity, strong electromagnetic shielding, and uniformly distributed stray light. *Opt Expr*, 15(3):790-796. https://doi.org/10.1364/OE.15.000790

Vorobyev OB, 2011. Quality factor of an antenna with closely spaced resonances. *IEEE Antenn Wirel Propag Lett*, 10:1216-1219. https://doi.org/10.1109/LAWP.2011.2173653

Wang HY, Lu ZG, Tan JB, 2016. Generation of uniform diffraction pattern and high EMI shielding performance by metallic mesh composed of ring and rotated sub-ring arrays. *Opt Expr*, 24(20):22989-23000. https://doi.org/10.1364/OE.24.022989

Wang HY, Lu ZG, Liu YS, et al., 2017. Double-layer interlaced nested multi-ring array metallic mesh for high-performance transparent electromagnetic interference

shielding. *Opt Lett*, 42(8):1620-1623. https://doi.org/10.1364/OL.42.001620

Wang HY, Lu ZG, Tan JB, et al., 2018. Transparent conductor based on metal ring clusters interface with uniform light transmission for excellent microwave shielding. *Thin Sol Films*, 662:76-82. https://doi.org/10.1016/j.tsf.2018.07.038

Wang WQ, Bai BF, Zhou Q, et al., 2018. Petal-shaped metallic mesh with high electromagnetic shielding efficiency and smoothed uniform diffraction. *Opt Mater Expr*, 8(11): 3485-3493. https://doi.org/10.1364/OME.8.003485

Wen B, Wang XX, Cao WQ, et al., 2014. Reduced graphene oxides: the thinnest and most lightweight materials with highly efficient microwave attenuation performances of the carbon world. *Nanoscale*, 6(11):5754-5761. https://doi.org/10.1039/C3NR06717C

Wu RY, Cui TJ, 2020. Microwave metamaterials: from exotic physics to novel information systems. *Front Inform Technol Electron Eng*, 21(1):4-26. https://doi.org/10.1631/FITEE.1900465

Wu ZC, Chen ZH, Du X, et al., 2004. Transparent, conductive carbon nanotube films. *Science*, 305(5688):1273-1276. https://doi.org/10.1126/science.1101243

Yamada T, Morizane T, Arimitsu T, et al., 2008. Application of low resistivity Ga-doped ZnO films to transparent electromagnetic interference shielding material. *Thin Sol Films*, 517(3):1027-1031. https://doi.org/10.1016/j.tsf.2008.06.047

Yang T, Hung CC, 2007. Multiple-attribute decision making methods for plant layout design problem. *Robot Comput-Integr Manuf*, 23(1):126-137. https://doi.org/10.1016/j.rcim.2005.12.002

Zeng XY, Zhang QK, Yu RM, et al., 2010. A new transparent conductor: silver nanowire film buried at the surface of a transparent polymer. *Adv Mater*, 22(40):4484-4488. https://doi.org/10.1002/adma.201001811

Zhang H, Gu CL, Gu LW, et al., 2011. The evaluation of tourism destination competitiveness by TOPSIS & information entropy—a case in the Yangtze River Delta of China. *Tour Manag*, 32(2):443-451. https://doi.org/10.1016/j.tourman.2010.02.007

Zhang XX, Ren AD, Liu Y, 2020. Decoupling methods of MIMO antenna arrays for 5G applications: a review. *Front Inform Technol Electron Eng*, 21(1):62-71. https://doi.org/10.1631/FITEE.1900466

Zhong H, Han Y, Lin J, et al., 2020. Pattern randomization: an efficient way to design high-performance metallic meshes with uniform stray light for EMI shielding. *Opt Expr*, 28(5):7008-7017. https://doi.org/10.1364/OE.386921

Zhu HX, Yang YQ, Sheng A, et al., 2019. Layered structural design of flexible waterborne polyurethane conductive film for excellent electromagnetic interference shielding and low microwave reflectivity. *Appl Surf Sci*, 469:1-9. https://doi.org/10.1016/j.apsusc.2018.11.007

Zhu M, Xiong CX, Lee Q, 2007. Research on ITO transparent electromagnetic shielding coatings for E-O system. Proc SPIE 6722, 3rd Int Symp on Advanced Optical Manufacturing and Testing Technologies: Advanced Optical Manufacturing Technologies, Article 67223Y. https://doi.org/10.1117/12.783569

Zou ZH, Yun Y, Sun JN, 2006. Entropy method for determination of weight of evaluating indicators in fuzzy synthetic evaluation for water quality assessment. *J Environ Sci*, 18(5):1020-1023. https://doi.org/10.1016/S1001-0742(06)60032-6

Yilei ZHANG, first author of this invited paper, received her BS degree in Automation from Guangxi University, Nanning, China. She is currently a PhD candidate at the Instrument Science and Technology from the Harbin Institute of Technology, Harbin, China. Her research interests include optical transparent electromagnetic shielding windows and tunable absorber.

Zhengang LU, corresponding author of this invited paper, received his BS and PhD degrees in Instrument Science and Technology from the Harbin Institute of Technology (HIT), Harbin, China. At present, he is a professor at the HIT, a vice director of the Center of Ultra-precision Optoelectronic Instrument Engineering, HIT. He is a corresponding expert of *Front Inform Technol Electron Eng*. His current research interests include micro-nano optics and electromagnetic shielding optical windows and precision instruments and engineering.

Jiubin TAN received his BS, MS, and PhD degrees in Instrument Science and Technology from the Harbin Institute of Technology (HIT), Harbin, China. He was elected as an Academician of the Chinese Academy of Engineering in 2017. He is now the president of the Precision Instrument Engineering Research Institute of the HIT, and the deputy director of the National Metrology Strategy Expert Advisory Committee. He is an editorial board member of *Front Inform Technol Electron Eng*. His current research interests include ultra-precision measurement technology and instrument engineering.